Acta Crystallographica Section A
Foundations of Crystallography
ISSN 0108-7673

Received 21 January 2002
Accepted 22 August 2002

Extinction effect and Borrmann effect of resonant dynamical scattering in the Bragg case

Tomoe Fukamachi,[a]* Riichirou Negishi,[a] ShengMing Zhou,[a] Masami Yoshizawa[a] and Takaaki Kawamura[b]

[a]Saitama Institute of Technology, 1690 Fusaiji, Okabe, Ohsato, Saitama 369-0293, Japan, and [b]Department of Physics, Yamanashi University, Kofu, Yamanashi 400-8510, Japan. Correspondence e-mail: tomoe@sit.ac.jp

In the Bragg case, X-ray beams suffer from anomalous absorption due to extinction effects without photo-absorption and are localized in the surface when X-ray total reflection occurs around an exact Bragg angle from a perfect crystal. On the other hand, the Borrmann effect due to anomalous transmission occurs in a thin perfect crystal with photo-absorption under a proper condition. There is a clear distinction between the extinction effect and the Borrmann effect. It is found that it is possible to separate the Borrmann effect from the extinction effect when the real part of the atomic scattering factor is zero. The calculated rocking curves agree well with the measured ones around the Ge *K*-absorption edge of the Ge 844 reflection.

1. Introduction

When X-rays are diffracted from a perfect crystal, several effects peculiar to such a diffraction, so-called dynamical effects, have been pointed out. Anomalous absorption and anomalous transmission, *i.e.* the Borrmann effect, is one of the typical examples. This effect has been interpreted in terms of the conventional theory of dynamical X-ray diffraction, in which Thomson scattering is primarily dealt with and the absorption is considered only as a perturbation. When resonant scattering becomes dominant, the scattering factor changes and a different form of dynamical effect can be expected. A theoretical study on nuclear resonant dynamical diffraction has been initiated by Kagan *et al.* (1968). In an experiment, an interesting effect is reported that the energy width of the diffracted wave is about ten times larger, *i.e.* the lifetime is ten times shorter, at a Bragg angle under resonance condition (Bürck *et al.*, 1990). The increased energy width is interpreted as a result of the coherent response of the nuclear ensemble. Theoretical studies on atomic resonant dynamical scattering have been done by Kato (1992) and by Fukamachi & Kawamura (1993) (hereafter referred as FK). According to the results, the angular width of rocking curves from a semi-infinite crystal becomes very small when the resonant scattering becomes dominant. FK have pointed out that the Borrmann effect occurs regardless of crystal thickness in the Laue case when only the resonant scattering contributes.

The atomic scattering factor can be expressed as $f = f^0 + f' + if''$, where f^0 is the normal atomic scattering factor for Thomson scattering, and f' and f'' are the real and imaginary parts of the anomalous scattering factor for resonant scattering, respectively. When the energy of an X-ray approaches an absorption edge of an atom, f' becomes negative and its absolute value increases. Consequently, the real part of f may vanish ($f^0 + f' = 0$), and only the imaginary part f'' remains non-zero. A scattering induced by f'' only has been observed experimentally (Fukamachi *et al.*, 1993). Although some interesting phenomena are expected at this condition, it is difficult to carry out an experiment to obtain a sharp diffracted peak as predicted by theory. Recently, X-ray topography of the GaAs 200 reflection near Ga and As *K*-absorption edges has been observed by Negishi *et al.* (2001). It is shown that lattice defect images change due to the resonant scattering. These results demonstrate that the topography by using atomic resonant scattering has a possible application to the observation of microstructure in a crystal.

In the Bragg case, when X-ray total reflection from a semi-infinite perfect crystal occurs around the Bragg angle, the X-ray wavevector in the crystal becomes complex even without absorption. The incident X-rays cannot penetrate deep into the crystal due to the imaginary part of the wavevector, *i.e.* the anomalous absorption results. This is called the extinction effect. For an absorbing crystal, the linear absorption coefficient μ becomes larger (anomalous absorption) or smaller (anomalous transmission) than the mean linear absorption coefficient μ_0 around the Bragg angle (James, 1948, 1963). The anomalous transmission is usually called the Borrmann effect (Borrmann, 1941).

In this paper, in order to understand how the extinction effect and the Borrmann effect occur, we investigate complex dispersion surfaces (Fukamachi *et al.*, 1995) according to a dynamical theory with atomic or nuclear resonant scattering, and compare the theoretical results with the measured ones.

2. Theoretical basis

2.1. X-ray polarizability

The Fourier coefficient χ_h of X-ray polarizability is usually expressed as

$$\chi_h = \chi_{hr} + i\chi_{hi} = |\chi_{hr}|\exp(i\alpha_{hr}) + i|\chi_{hi}|\exp(i\alpha_{hi}). \quad (1)$$

The real and imaginary parts are given by

$$\chi_{hr} = -\frac{4\pi}{V\omega^2}\sum_j (f_j^0 + f_j')\exp(i\mathbf{h}\cdot\mathbf{r}_j)T_j, \quad (2a)$$

$$\chi_{hi} = -\frac{4\pi}{V\omega^2}\sum_j f_j''\exp(i\mathbf{h}\cdot\mathbf{r}_j)T_j, \quad (2b)$$

using atomic units ($\hbar = e = m = 1$). Here V is the unit-cell volume, $\mathbf{h}$ a reciprocal-lattice vector, $\mathbf{r}_j$ the position vector of an atom j and T_j a factor for temperature correction.

Let us put

$$\chi_h\chi_{-h} = \bar{\chi}_h^2(u + iv), \quad (3)$$

with

$$\bar{\chi}_h = (|\chi_{hr}|^2 + |\chi_{hi}|^2)^{1/2}, \quad (4)$$

$$u = (|\chi_{hr}|^2 - |\chi_{hi}|^2)/\bar{\chi}_h^2, \quad (5)$$

$$v = (1 - u^2)^{1/2}\cos\delta \quad (6)$$

and

$$\delta = \alpha_{hi} - \alpha_{hr}. \quad (7)$$

If atomic resonant scattering is ignored and only Thomson scattering is considered, we obtain $\chi_{0i} = \chi_{hi} = 0$ and $u = 1$. In fact, this condition cannot be satisfied in an actual monoatomic crystal. However, $u = 1$ is satisfied near an absorption edge in a polyatomic crystal even for $\chi_{0i} \neq 0$, which has been confirmed by Fukamachi *et al.* (1996). The condition $u = -1$ is satisfied near an absorption edge even in a monoatomic crystal when $f^0 + f' = 0$.

According to the above notation, the parameters u and v vary from -1 to 1 continuously, therefore $u + iv$ form the unit circle in a complex plane. When the condition of $|\chi_h| = |\chi_{-h}|$ is satisfied, δ is either 0 or π, so $u + iv$ is always located in the circumference of the unit circle. When the condition of $|\chi_h| \neq |\chi_{-h}|$ is satisfied, $u + iv$ is located at a point inside the unit circle.

The conventional theory is applicable only to the condition $|\chi_{hi}|/|\chi_{hr}| \leq 0.1$ (Zachariasen, 1945), namely $1 \geq u \geq 0.98$. Under such a condition, the dispersion surface calculated by the two-wave approximation is a hyperbola. However, the shape of the dispersion surface changes greatly for other values of u and v, which is investigated below.

2.2. Complex dispersion surface

In order to understand the physical meaning of the complex dispersion surface, we begin with investigating the basic equation of diffraction in the two-wave approximation. The dispersion surface is given by

$$\xi_0\xi_h = (P^2\kappa_{0r}^2/4)\chi_h\chi_{-h}, \quad (8)$$

where P is the polarization factor and $P = 1$ for σ polarization and $P = |\cos 2\theta_B|$ for π polarization (here θ_B is the Bragg angle in vacuum). ξ_0 and ξ_h can be put in the form

$$\xi_0 = (\mathbf{k}_0^2)^{1/2} - \kappa_0, \quad \xi_h = (\mathbf{k}_h^2)^{1/2} - \kappa_0, \quad (9)$$

where $\mathbf{k}_0$ and $\mathbf{k}_h$ ($|\mathbf{k}_0| = |\mathbf{k}_h| = 2\pi/\lambda$, λ is the wavelength) are the wavevectors for the incident and diffracted waves in the crystal, respectively. κ_0 is the average wave number in the crystal and can be written as

$$\kappa_0 = \kappa_{0r} + i\kappa_{0i} \quad (10)$$

with

$$\kappa_{0r} = K(1 + \chi_{0r}/2), \quad \kappa_{0i} = K\chi_{0i}/2, \quad (11)$$

where K is the wave number in vacuum. The mean absorption coefficient μ_0 can be expressed as

$$\mu_0 = -\kappa_{0i}/2 = K\chi_{0i}. \quad (12)$$

According to

$$\mathbf{k}_0 = \mathbf{k}_{0r} + i\mathbf{k}_{0i}, \quad \mathbf{k}_h = \mathbf{k}_{0r} + \mathbf{h} + i\mathbf{k}_{0i} = \mathbf{k}_{hr} + i\mathbf{k}_{0i} \quad (13)$$

and considering the condition $|\mathbf{k}_{0r}| \gg |\mathbf{k}_{0i}|$ for X-rays, we can put

$$\mathbf{k}_0^2 = \mathbf{k}_{0r}^2 + 2i\mathbf{k}_{0r}\cdot\mathbf{k}_{0i}. \quad (14)$$

If we put $\mathbf{s}_0 = \mathbf{k}_{0r}/|\mathbf{k}_{0r}|$ and $\mathbf{s}_h = \mathbf{k}_{hr}/|\mathbf{k}_{hr}|$,

$$(\mathbf{k}_0^2)^{1/2} = |\mathbf{k}_{0r}| + i\mathbf{s}_0\cdot\mathbf{k}_{0i}, \quad (\mathbf{k}_h^2)^{1/2} = |\mathbf{k}_{hr}| + i\mathbf{s}_h\cdot\mathbf{k}_{hi}. \quad (15)$$

Then from (9), (10) and (15), we obtain

$$\xi_0 = |\mathbf{k}_{0r}| - \kappa_{0r} + i(\mathbf{s}_0\cdot\mathbf{k}_{0i} - \kappa_{0i}) = \xi_{0r} + i\xi_{0i}, \quad (16a)$$

$$\xi_h = |\mathbf{k}_{hr}| - \kappa_{0r} + i(\mathbf{s}_h\cdot\mathbf{k}_{hi} - \kappa_{0i}) = \xi_{hr} + i\xi_{hi}. \quad (16b)$$

Because κ_0 is complex, it is necessary to draw a dispersion surface in a complex plane. By replacing κ_0 by κ_{0r}, we obtain

$$\xi_0 = (\mathbf{k}_0^2)^{1/2} - \kappa_{0r} - i\kappa_{0i} = \xi_0' - i\kappa_{0i}, \quad (17a)$$

$$\xi_h = (\mathbf{k}_h^2)^{1/2} - \kappa_{0r} - i\kappa_{0i} = \xi_h' - i\kappa_{0i}. \quad (17b)$$

Equation (8) can be rewritten as

$$(\xi_0' - i\kappa_{0i})(\xi_h' - i\kappa_{0i}) = (P^2\kappa_{0r}^2/4)\bar{\chi}_h^2(u + iv) \quad (18)$$

with the relations

$$\xi_0' = \xi_{0r}' + i\xi_{0i}', \quad \xi_{0r}' = \xi_{0r}, \quad \xi_{0i}' = \mathbf{s}_0\cdot\mathbf{k}_{0i}, \quad (19a)$$

$$\xi_h' = \xi_{hr}' + i\xi_{hi}', \quad \xi_{hr}' = \xi_{hr}, \quad \xi_{hi}' = \mathbf{s}_h\cdot\mathbf{k}_{0i}. \quad (19b)$$

We use the Cartesian coordinate to draw the dispersion surface and take the X axis parallel to the crystal surface. Using

$$Y_0 = Y_{0r} + iY_{0i}, \quad (20)$$

we obtain

$$\xi_{0r}' = X_0\sin\theta_1 + Y_{0r}\cos\theta_1, \quad \xi_{0i}' = Y_{0i}\cos\theta_1, \quad (21a)$$

$$\xi_{hr}' = X_0\sin\theta_2 + Y_{0r}\cos\theta_2, \quad \xi_{hi}' = Y_{0i}\cos\theta_2, \quad (21b)$$

where θ_1 and θ_2 are the same as in Fukamachi *et al.* (1995). Using the excitation error defined as (FK),

$$W = -\frac{X_0 \sin 2\theta'_B}{|\cos\theta_1 \cos\theta_2|^{1/2}\kappa_{0r} P\bar{\chi}_h}. \quad (22)$$

In the Bragg case ($\cos\theta_2 < 0$), we get

$$Y_{0r} = \frac{-\kappa_{0r} P\bar{\chi}_h}{2|\cos\theta_1 \cos\theta_2|^{1/2}}\left[\frac{\sin 2\beta}{\sin 2\theta'_B} W \pm \mathrm{Re}\{A-B\}^{1/2}\right], \quad (23a)$$

$$Y_{0i} = \frac{-\kappa_{0r} P\bar{\chi}_h}{2|\cos\theta_1 \cos\theta_2|^{1/2}}\left[g\frac{\cos\theta'_B \sin\beta}{|\cos\theta_1 \cos\theta_2|^{1/2}} \pm \mathrm{Im}\{A-B\}^{1/2}\right]. \quad (23b)$$

Here θ'_B is a Bragg angle in the crystal,

$$A = (W + ig')^2, \quad B = u + iv \quad (24)$$

and

$$g = \frac{\chi_{0i}}{P\bar{\chi}_h}, \quad g' = g\frac{\sin\theta'_B \cos\beta}{|\cos\theta_1 \cos\theta_2|^{1/2}}, \quad (25)$$

where β is the same as in Fukamachi *et al.* (1995).

According to the diffraction condition, the dispersion point can be given as the crossing point on the dispersion surface with the normal line ν, so ξ_0 and ξ_h can be determined. The electric field D_0 related to the incident wave and D_h related to the diffracted wave in the crystal can be given as follows:

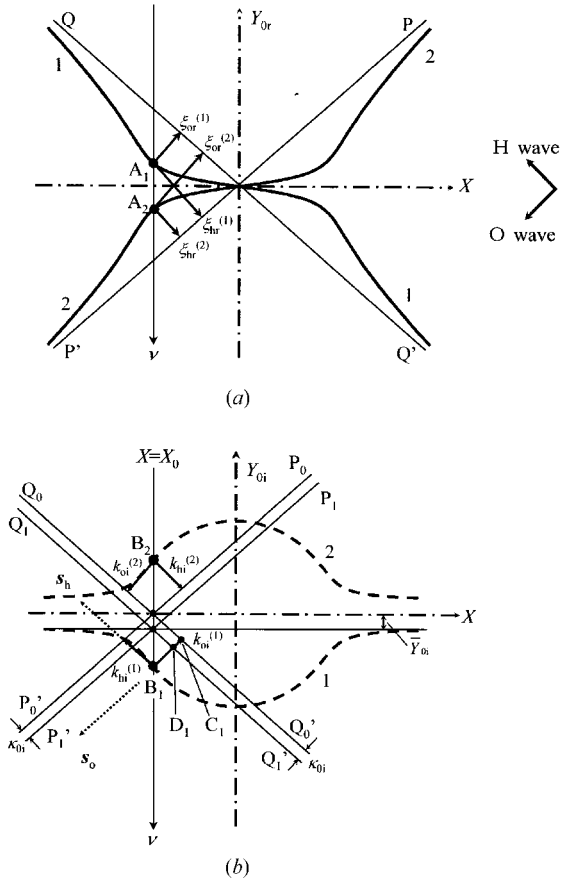

Figure 1
The complex dispersion surface when $u = 1$ ($\chi_{0i} \neq 0$) in the Bragg case. The thick solid curves represent the real part (a), and the thick dashed curves the imaginary part (b).

$$D_0 = \frac{\kappa_{0r}}{2\xi_0} P\chi_{-h} D_h = \frac{2\xi_h}{\kappa_{0r}}\frac{1}{P\chi_h} D_h. \quad (26)$$

Now we discuss the physical content of the obtained complex dispersion surface. Fig. 1 shows the dispersion surface in the symmetric Bragg case for $u = 1$ which includes the resonant scattering. The thick solid curves (a) represent the real part, and the thick dashed curves (b) represent the imaginary part. The physical content of the real part is well explained in conventional dynamical theory and here we focus on the physical meaning of the imaginary part.

The dispersion points are marked A_1 and A_2 for the real part, and B_1 and B_2 for the imaginary part, respectively. The line $Q_0Q'_0$ is perpendicular to $\mathbf{s}_0$ and is the section of the surface $\mathbf{s}_0 \cdot \mathbf{k}_{0i}$ expressed by (15). The line $P_0P'_0$ is the section of the surface $\mathbf{s}_h \cdot \mathbf{k}_{0i}$ and is perpendicular to $\mathbf{s}_h$. These sections, which are parallel to the corresponding asymptotes QQ' and PP', represent the same amount of absorption in the crystal. The vector B_1C_1 corresponds to $\mathbf{k}_{0i}^{(1)}$ and the segment B_1C_1 is equal to $\xi_{0i}^{\prime(1)}$. Furthermore, $Q_1Q'_1$ is an interface formed by moving $\mathbf{s}_0 \cdot \mathbf{k}_{0i}$ along the O direction by κ_{0i}, the intersection point between $Q_1Q'_1$ and its perpendicular line through B_1 is D_1, and then $B_1D_1 = \xi_{0i}^{\prime(1)} - \kappa_{0i} = \xi_{0i}^{(1)}$ is obtained.

The intensity of the j branch wave at depth z is proportional to

$$|\exp(-ik_{0z}^{(j)} z)|^2 = \exp(2Y_{0i}^{(j)} z), \quad (27)$$

where the relation $k_{0z}^{(j)} = \kappa_{0r}/\sin\theta'_B + Y_{0r}^{(j)} + iY_{0i}^{(j)}$ is used. The linear absorption coefficient $\mu^{(j)}$ can be written as

$$\mu^{(j)} = -2Y_{0i}^{(j)} \sin\theta'_B = -2k_{0i}^{(j)}. \quad (28)$$

In the limit of $|X_0| \to \infty$, Y_{0i} of the lower branch becomes $\bar{Y}_{0i}$. From Fig. 2, $\bar{Y}_{0i}$ is given by

$$\bar{Y}_{0i} = Y_{0i}(|X_0| \to \infty) = \kappa_{0i}/\sin\theta'_B \quad (29)$$

and

$$\mu_0 = -2\bar{Y}_{0i} \sin\theta'_B = -2\kappa_{0i}. \quad (30)$$

We define

$$\mu_a^{(j)} = \mu^{(j)} - \mu_0 = -2\xi_{0i}^{(j)}, \quad (31)$$

which is called the abnormal absorption coefficient hereafter.

2.3. Extinction effect and Borrmann effect

For investigating the characteristics of the extinction effect and the Borrmann effect, complex dispersion surfaces are shown for (a) $(u, v) = (1, 0)$, (b) $(u, v) = (-1, 0)$, (c) $(u, v) = (0, 1)$ and (d) $(u, v) = (0, -1)$, in the symmetric Bragg case in Fig. 2.

According to the imaginary part of the dispersion surface for $u = 1$ shown in Fig. 1(b) and Fig. 2(a), the lower branch wave suffers anomalous absorption because $\xi_{0i} < 0$ and $\mu_a > 0$, then $\mu > \mu_0$ is satisfied, and the upper branch wave suffers anomalous transmission because $\xi_{0i} > 0$ and $\mu_a < 0$. The phenomenon of the anomalous absorption and the anomalous transmission caused by χ_{hr} is called the extinction effect in this paper as it occurs even without photo-absorption. Figs. 3(a)

and (*b*) show $|D_0^{(j)}/E_0|$ and $|D_0^{(j)}\exp(-ik_{0z}^{(j)}z)/E_0|$ under the conditions (*a*) $u = 1$, $\chi_{0i} = 0$ and $W = 0$, and (*b*) $u = -1$ and $W = 0$. In Fig. 3(*a*), though $|D_0^{(1)}/E_0| > |D_0^{(2)}/E_0|$, $|D_0^{(j)}\exp(-ik_{0z}^{(j)}z)/E_0|$ has the same value for different branches and is localized in the surface. Thus, the intensity of a transmitted rocking curve calculated by using the formula derived by Negishi *et al.* (1998) becomes weak around a Bragg condition due to the extinction effect as shown in Fig. 4(*a*). When such an extinction effect is generated, $|\mathbf{k}_{0i}^{(j)}| > |\kappa_{0i}|$ holds as shown in the imaginary dispersion surface.

The imaginary dispersion surface for $u = -1$ in Fig. 2(*b*) shows that the lower and upper branches with $\xi_{0i} > 0$ and $\mu_a < 0$ mean the anomalous transmission. When $k_{0iz}^{(j)} = 0$ at $W = 0$, $|D_0^{(j)}\exp(-ik_{0z}^{(j)}z)/E_0|$ has the same value as $|D_0^{(j)}/E_0|$ and $|D_0^{(1)}|$ is larger than $|D_0^{(2)}|$ as shown Fig. 3(*b*). Then the peak of the transmitted rocking curve in Fig. 4(*b*) is caused by the anomalous transmission mainly due to branch 1. The phenomenon of anomalous transmission caused by χ_{hi} is called the Borrmann effect in this paper. When the effect is generated, $|\mathbf{k}_{0i}^{(j)}| < |\kappa_{0i}|$ holds as shown in the imaginary dispersion surface.

The imaginary dispersion surfaces for $(u, v) = (0, 1)$ and $(0, -1)$ are shown in Figs. 2(*c*) and (*d*), respectively. It can be understood in Fig. 2(*c*) that the anomalous transmission is generated due to the Borrmann effect for $X > 0$ and that the anomalous absorption is generated due to the extinction effect for $X < 0$. As the dispersion surfaces for $v = -1$ are obtained by reversing those for $v = 1$ around $X = 0$, similar effects are obtained for $v = -1$. Fig. 4(*c*) shows the transmitted rocking curves for $(u, v) = (0, 1)$ and $(0, -1)$. When $(u, v) = (0, 1)$, the peak located at the negative side of W results from the anomalous transmission due to the Borrmann effect and the valley located in the positive side of W results from the anomalous absorption due to the extinction effect. The reverse trend of the peak and valley positions with respect to $W = 0$ can be observed between $v = -1$ and $v = 1$.

2.4. Simulation

Because the abnormal absorption coefficient $\mu_a < 0$ always holds when $u = -1$ in the Bragg case, anomalous transmission is expected due to the Borrmann effect regardless of the crystal thickness. Here, we analyze the condition $u = -1$ theoretically in an actual crystal, *i.e.* near the Ge *K*-absorption edge of the Ge 844 reflection.

In Fig. 5, the locus of f is given as ω changes where the abscissa represents $f^0 + f'$ and the ordinate represents f''. ω_K is the energy of the Ge *K*-absorption edge (11103 eV). We note that $f^0 + f' = 0$ is satisfied at $\omega = \omega_K \pm 1.3$ eV and only f'' remains non-zero, namely, $u = -1$ holds. In the energy region of $\omega_K - 1.3 < \omega < \omega_K + 1.3$ eV, $v < 0$ holds due to $f^0 + f' < 0$ (outside the energy region, $v > 0$). In Fig. 6, the rocking curves of Ge 844 with crystal thickness 80 µm are shown, at the energy points (*a*) $\omega = \omega_K - 4.3$ eV, (*b*) $\omega = \omega_K - 1.3$ eV and (*c*) $\omega = \omega_K - 0.5$ eV, respectively. The corresponding values of (u, v) are (0.40, 0.91) for Fig. 6(*a*), (−1, 0) for 6(*b*) and (−0.83, −0.56) for 6(*c*). The shapes of the diffracted rocking curves (thin solid curves) for Figs. 6(*a*)–(*c*)

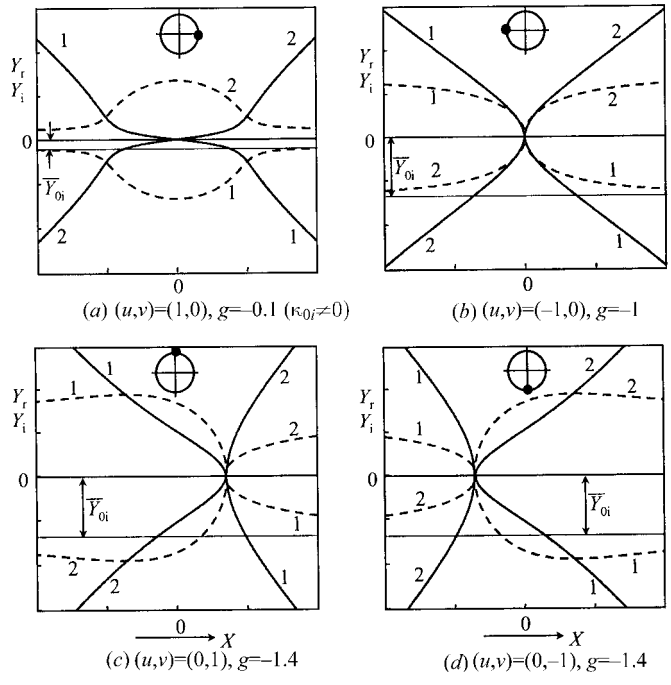

Figure 2
Complex dispersion surfaces in the Bragg case for (*a*) $(u, v) = (1, 0)$, (*b*) $(u, v) = (-1, 0)$, (*c*) $(u, v) = (0, 1)$ and (*d*) $(u, v) = (0, -1)$. The thick solid curves represent the real part, and the dashed curves the imaginary part.

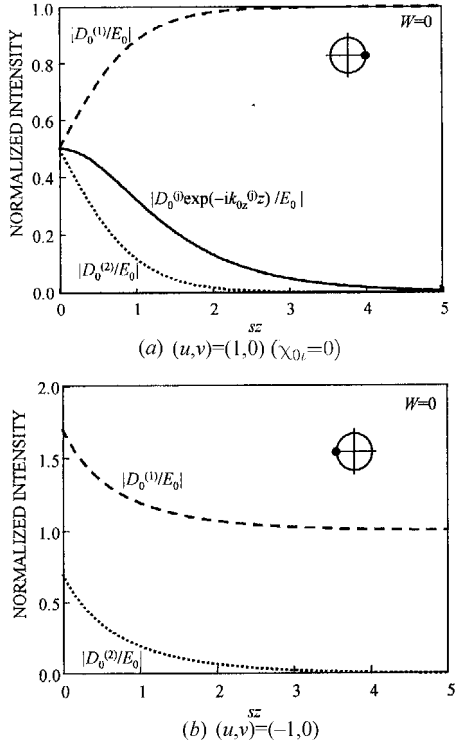

Figure 3
The electric fields $|D_0^{(j)}/E_0|$ and $|D_0^{(j)}\exp(-ik_{0z}^{(j)}z)/E_0|$ in the crystal when $W = 0$. E_0 is the electric field of the incident X-ray. (*a*) $(u, v) = (1, 0)$ and $\chi_{0i} = 0$, and (*b*) $(u, v) = (-1, 0)$.

are almost the same with a peak located in the center. In fact, except for Fig. 6(*b*), the peak deviates slightly from the center in 6(*a*) and 6(*c*), and locates in the negative angle side in 6(*a*), and in the positive angle side in 6(*c*). However, the corresponding transmitted rocking curves (thick solid curves) in Figs. 6(*a*)–(*c*) change remarkably. In Fig. 6(*b*), the anomalous transmission peak in the center due to the Borrmann effect appears in the background after suffering from the average absorption. In Fig. 6(*a*), the peak can be seen in the negative angle side due to the anomalous transmission of the Borrmann effect, and the valley can be seen in the positive angle side due to the extinction effect. But in Fig. 6(*c*), the reversed variation with respect to 6(*a*) is seen.

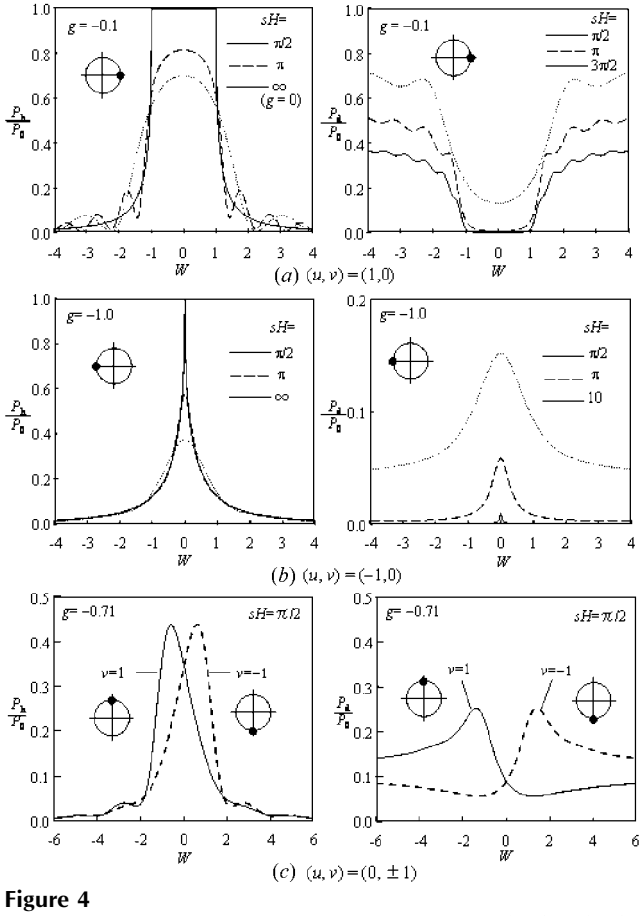

Figure 4
Rocking curves in the symmetric Bragg case. (*a*) $(u, v) = (1, 0)$, (*b*) $(u, v) = (-1, 0)$ and (*c*) $(u, v) = (0, 1)$ and $(u, v) = (0, -1)$. P_h/P_0 represents the normalized diffraction intensity, and P_d/P_0 the normalized transmitted one. The parameter sH is proportional to the crystal thickness.

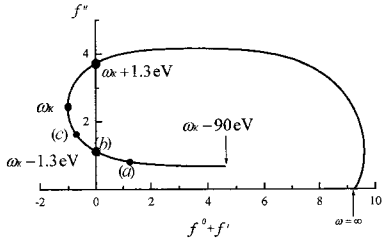

Figure 5
The locus of f for Ge 844. Values of f' and f''obtained by the Parratt & Hempstead (1954) method using oscillator strength from Cromer's table (Cromer, 1965).

3. Experiment

According to the above theoretical analysis, the extinction effect and the Borrmann effect coexist in the region of $1 > u > -1$, while only the extinction effect exists for $u = 1$ and only the Borrmann effect for $u = -1$. We have obtained the experimental result for the condition that only the extinction effect exists for $u = 1$ (Negishi *et al.*, 1998). In the present work, we performed an experiment to examine the theoretical conclusion that only the Borrmann effect exists for $u = -1$.

The schematic diagram of the measuring system is shown in Fig. 7. The experiment was carried out on beamline 15C at KEK-PF. The X-ray from SR was monochromated by using an Si 111 double-crystal monochromator and an Si 664 monochromator. The diffracted and transmitted rocking curves of

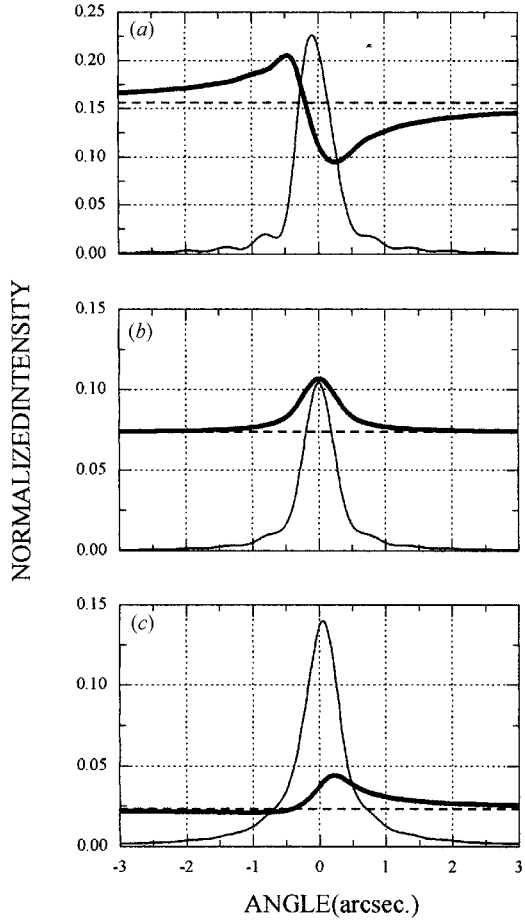

Figure 6
Calculated rocking curves of Ge 844 near the Ge K-absorption edge at (*a*) 4.3 eV, (*b*) 1.3 eV and (*c*) 0.5 eV below the edge. The thick solid curves represent the transmitted rocking curves and the thin solid curves the diffracted one. The dashed lines represent the transmitted intensity assuming the mean absorption. The sample thickness is 80 μm and the temperature factor B = 0.58 Å^2.

Ge 844 were measured from a crystal with thickness 82 μm with an etch-pit density (EPD) value less than 500 cm^{-1}. Fig. 8 shows the measured rocking curves. The angle in each figure is normalized so that a peak of the diffracted rocking curve is in the center. The energy of the X-rays was calibrated by measurement of XANES with a thin Ge plate with a precision ±0.5 eV. According to the previous experimental results of Fukamachi *et al.* (1993) for Ge 844, $u = -1$ is satisfied at $\omega_K - 2.8 \pm 0.2$ eV but not at $\omega_K - 1.3$ eV as predicted by the theory. With this in mind, the measured rocking curves at energy points (*a*) $\omega_K - 4$ eV, (*b*) $\omega_K - 3$ eV and (*c*) $\omega_K - 2$ eV are shown in Fig. 8.

4. Results and discussion

In the Bragg case, James (1948, 1963) investigated the anomalous absorption due to the extinction effect in the region around $|\chi_{hi}|/|\chi_{hr}| \cong 0.1$ using the conventional dynamical theory with absorption. By use of Cu $K\alpha$ X-rays, he obtained the result that μ is 25 times larger than μ_0 for NaCl 200 at $W = 0$. However, he did not further investigate the origins that lead to $\mu < \mu_0$.

In the present studies, the origins of the anomalous absorption and the anomalous transmission corresponding to the extinction effect and the anomalous transmission corresponding to the Borromann effect have been shown by using the complex dispersion surface. It is concluded that: (i) only the extinction effect, which is the dynamical effect resulting from χ_{hr}, is generated for $u = 1$; (ii) only the Borrmann effect, which is the dynamical effect resulting from χ_{hi}, is generated for $u = -1$; and (iii) the extinction effect and the Borrmann effect coexist for $1 > u > -1$ except when $(u, v) = (0, 0)$. [For the condition $(u, v) = (0, 0)$, we do not expect the dynamical effect because the dispersion surface corresponds to the asymptote.] These effects are also reflected in the transmitted rocking curves as: (i) a valley for $u = 1$; (ii) a peak for $u = -1$; and (iii) a peak in the negative W side and a valley in the positive W side for $1 > u > -1$ and $v > 0$, or a peak in the positive side and a valley in the negative side for $1 > u > -1$ and $v < 0$. Here we emphasize that the Borrmann effect vanishes completely and only the extinction effect appears for $u = 1$ which may include the photo-absorption, and that the extinction effect vanishes completely and only the Borrmann effect appears for $u = -1$ in the Bragg case.

For $u \approx 1$, the valley due to anomalous absorption related only to the extinction effect has been observed by Negishi *et al.* (1998), which can be seen in the transmitted rocking curves of (*a*)–(*c*) in Fig. 5 in their paper. They tuned the X-ray energy to the points (*a*) 9 eV, (*b*) 6 eV and (*c*) 3 eV below the Ga *K*-absorption edge (10368 eV) for the GaAs 600 reflection. The measured transmitted rocking curve (*b*) shows a valley caused only by anomalous absorption due to the extinction effect. For $u \approx -1$, the systematic change has been seen clearly in the transmitted rocking curves as shown in Figs. 8(*a*)–(*c*). The peak of the transmitted rocking curve of Fig. 8(*b*) appears in the center. According to the theoretical analysis, this experimental result suggests that $u = -1$ is satisfied and only the anomalous transmission of the Borrmann effect occurs. Furthermore, the peak located in the low-angle side of Fig. 8(*a*) and that in the high-angle side of 8(*c*) results from the anomalous transmission of the Borrmann effect, which can be understood by comparing them with the theoretical results in Fig. 6. On the other hand, the valley located in the high-angle side of Fig. 8(*a*) and that in the low-angle side of 8(*c*) is generated by the anomalous absorption of

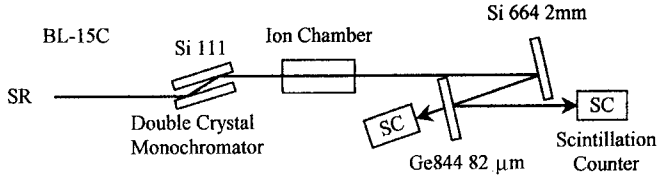

Figure 7
Schematic diagram of the measuring system.

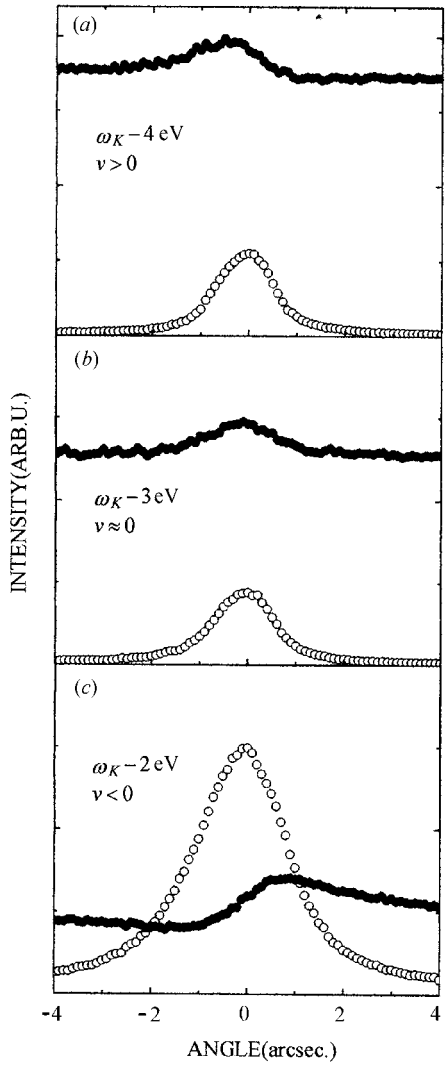

Figure 8
Observed rocking curves of Ge 844 near the Ge *K*-absorption edge. The closed circles represent the transmitted rocking curves and the open circles the diffracted ones. (*a*) 4 eV, (*b*) 3 eV and (*c*) 2 eV below the edge.

the extinction effect. Therefore, we come to a conclusion that asymmetric transmitted rocking curves appear due to the coexistence of the extinction effect and the Borrmann effect. The extinction effect is dominant in the high-angle side of the curve in Fig 8(*a*) and the low-angle side of curve 8(*c*), and the Borrmann effect is dominant in the low-angle side of curve 8(*a*) and the high-angle side of curve 8(*c*).

Under the extinction effect condition, X-rays are quite localized at a crystal surface and give rise to information on the surface. On the other hand, under the Borrmann effect condition without the extinction effect, X-rays propagate much deeper into the crystal than estimated by the mean absorption. We can vary the penetration depth of X-rays continuously by changing the energy under resonant condition. As an application, this may be used to obtain defect contrasts of X-ray topography at various depths by just changing X-ray energy, which will be our future work.

The complex dispersion surface obtained in the present paper can be used for any values of the scattering factors, *i.e.* $u + iv$ ($-1 \leq u \leq 1$) although that of the conventional theory is only applicable when the imaginary part of the scattering factors is small ($u \approx 1$). Thus the complex dispersion surface is expected to be very useful in the analysis of the experimental results of the atomic or nuclear resonant scattering. In addition, the formula (8) can be rewritten as follows:

$$(\xi_{0r}\xi_{hr} - \xi_{0i}\xi_{hi}) + i(\xi_{0r}\xi_{hi} + \xi_{hr}\xi_{0i}) = (P^2\kappa_{0r}^2/4)\bar{\chi}_h^2(u + iv). \tag{32}$$

In the main discussion about dynamical effects in the conventional dynamical theory (Batterman & Cole, 1964), the approximation of $|\xi_{0r}\xi_{hr}| \gg |\xi_{0i}\xi_{hi}|$ was adopted. It is clear that such an approximation is inadequate as shown in Figs. 1 and 2, where $|\xi_{0r}\xi_{hr}| \approx |\xi_{0i}\xi_{hi}|$.

The authors are particularly indebted to Professor M. Tokonami of Saitama Institute of Technology (SIT) for his valuable discussions, and are grateful to Professor H. Kawata, Dr K. Hirano, Dr X. Zhang and Dr I. Matsumoto of the Photon Factory for their help in the experiments. The experiments were carried out with the approval of the Photon Factory Committee, Proposal No. 2000G046. This work was financially supported by the Advanced Science Research Laboratory of SIT. One of authors (RN) was supported by a Grant-in-Aid (No. 12650018) for Scientific Research from the Ministry of Education, Culture, Sports, Science and Technology.

References

Batterman, B. W. & Cole, H. (1964). *Rev. Mod. Phys.* **36**, 681–717.
Borrmann, G. (1941). *Phys. Z.* **42**, 157–162.
Bürck, U., Smirnov, D. V., Mössbauer, R. L. & Hertrich, T. (1990). *J. Phys. Condens. Matter*, **2**, 3989–3995.
Cromer, D. T. (1965). *Acta Cryst.* **18**, 17–23.
Fukamachi, T. & Kawamura, T. (1993). *Acta Cryst.* A**49**, 384–388.
Fukamachi, T., Negishi, R. & Kawamura, T. (1995). *Acta Cryst.* A**51**, 253–258.
Fukamachi, T., Negishi, R., Yoshizawa, M., Ehara, K., Kawamura, T., Nakajima, T. & Zhao, Z. (1993). *Acta Cryst.* A**49**, 573–575.
Fukamachi, T., Negishi, R., Zhou, S., Yoshizawa, M., Sakamaki, T., Kawamura, T. & Nakajima, T. (1996). *Acta Cryst.* A**52**, 669–674.
James, R. W. (1948). *The Optical Principles of the Diffraction of X-rays*. London: G. Bell and Sons.
James, R. W. (1963). *Solid State Phys.* **15**, 53–220.
Kagan, Yu., Afanas'ev, A. M. & Perstnev, I. P. (1968). *Sov. Phys. JETP*, **27**, 819–824.
Kato, N. (1992). *Acta Cryst.* A**48**, 829–834.
Negishi, R., Fukamachi, T., Yoshizawa, M., Zhou, S., Xu, Z., Kawamura, T., Matsumoto, I., Sakamaki, T. & Nakajima, T. (1998). *J. Appl. Cryst.* **31**, 351–355.
Negishi, R., Yoshizawa, M., Zhou, S., Matsumoto, I., Fukamachi, T. & Kawamura, T. (2001). *Jpn J. Appl. Phys.* **40**, L884–L887.
Parratt, L. G. & Hempstead, C. F. (1954). *Phys. Rev.* **94**, 1593–1600.
Zachariasen, W. H. (1945). *Theory of X-ray Diffraction in Crystals*. New York: John Wiley and Sons.